Available online at www.sciencedirect.com

ScienceDirect

Procedia Structural Integrity 56 (2024) 82–89

Structural Integrity Procedia

www.elsevier.com/locate/procedia

Structural Integrity and Reliability of Advanced Materials obtained through Additive Manufacturing (SIRAMM23)

Additive manufacturing for orthopedic implants: morphological and material characterization of SLM thin Ti6Al4V samples

Francesca Danielli[a], Francesca Berti[a], Adelaide Nespoli[b], Valentina Lo Presti[a], Edoardo Sironi[a], Davide Ninarello[a,b], Tomaso Villa[a], Lorenza Petrini[c]*

[a]*LaBS-Laboratory of Biological Structure Mechanics – Department of Chemistry, Materials and Chemical Engineering "Giulio Natta", Politecnico di Milano, Piazza Leonardo da Vinci 32, Milano 20133, Italy*

[b]*National Research Council, Institute of Condensed Matter Chemistry and Technologies for Energy, Via Previati 1/E, Lecco 23900, Italy*

[c]*Department of Civil and Environmental Engineering", Politecnico di Milano, Piazza Leonardo da Vinci 32, Milano 20133, Italy*

Abstract

In the last decades, the orthopedic industry has increasingly adopted Additive Manufacturing (AM) technologies, such as selective laser melting, to produce custom devices. Given their novelty with respect to discrete-size implants, New 2017/745 Medical Device Regulation introduced the need for safety and quality demonstration of such unique devices, a non-trivial task since no defined criteria state how to test them. In this scenario, numerical analyses can be a robust tool for the intended purposes as long as the reliability of the numerical models is verified in terms of geometry reconstruction and material assignment. The latter need has to deal with the peculiarities of AM in the production of lattice structures, distinctive features of this new generation of devices conceived to mimic bone morphology. Indeed, the struts of such structures have diameters of hundreds of microns, which approach AM accuracy limit. If, on the one hand, the issues related to AM production are well-known, on the other hand, it is not yet fully understood how to deal with them if thin struts are manufactured. Given the still questionable research area and starting from the few literature findings, this study aims to provide an exhaustive morphological and material characterization of Ti6Al4V thin struts produced by selective laser melting, supporting experimental activities with numerical analyses. The importance of investigating together their morphology and mechanical behavior will be highlighted: morphological analyses will constitute the first step to assess the quality of the manufactured samples and to correctly interpret the experimental results of static and fatigue tests. In this light, the differences with respect to the mechanical properties of both machined samples and thick AM samples will be outlined. The outcomes of this research will be fundamental for the development of reliable FE models of lattice-based devices.

* Corresponding author. Tel.: +39 02 2399 4307; fax: +39 02 2399 4286.
E-mail address: lorenza.petrini@polimi.it

2452-3216
10.1016/j.prostr.2024.02.041

Keywords: Fatigue tests; Finite element analysis; Morphological analyses; Selective laser melting; Static tests; Thin struts; Ti6Al4V ELI

1. Introduction

Nowadays, the advantages of AM applied to the orthopedic industry are well recognized. The production of a new generation of custom devices is an outstanding example: lattice structures are conceived both to design lightweight implants, reducing the risk of stress-shielding, and to mimic the trabecular bone, enhancing the implant osteointegration within the surrounding bone tissue. These devices are commonly produced using Selective Laser Melting (SLM) as a manufacturing process and Ti6Al4V alloys as metallic powder. Contrary to traditional manufacturing processes, such as machining, AM allows the production of custom devices fitting complex anatomies. Unlike discrete-size devices, there are no defined methodologies to assess the safety and quality of custom implants, given their unique shapes and dimensions. Finite Element (FE) modeling of implantable devices is a viable option as long as the FE model reliability is verified in terms of geometry reconstruction and assignment of material properties. As for the latter, the characterization of the struts involved in the implants' lattice structures is still an open issue and is hindered by their dimensions approaching the accuracy limit of AM technologies. For instance, the minimum printable strut diameter is about 200 μm (Yang et al., 2021). Therefore, uncertainties in their manufacturing arise, affecting the final product morphology and mechanical properties. Internal and surface defects (e.g., porosity and surface roughness) may be present, and their effect on the material properties is particularly relevant, given the struts dimensions in the order of hundreds of microns. Recent works (Hossain et al., 2021; Murchio et al., 2021a) highlighted a significant discrepancy between thin struts and samples with dimensions in the order of centimeters or bigger. The reasons behind these findings are many and not yet fully understood, making this field still open to further investigations. Given the introduced evidence, morphology and mechanical behavior (both static and fatigue) of AM thin struts should be investigated together. As for the fatigue behavior, if its characterization has been exhaustively conducted on traditional manufacturing Ti6Al4V, the same cannot be stated for AM samples. The emerging literature findings assess that the fatigue life of AM materials is lower with respect to the conventional ones due to, for instance, internal and surface defects introduced by AM (Edwards & Ramulu, 2014; Greitemeier et al., 2016; Nakatani et al., 2019; Pegues et al., 2018; Persenot et al., 2019). However, to the best of the authors' knowledge, the majority of literature works deal with samples having dimensions in the order of centimeters (e.g., diameter>3mm), but very few works (Murchio et al., 2021a) have investigated smaller samples (e.g. diameter <1mm), object of the current work. Thus, this study aims to provide an exhaustive morphological and material characterization of Ti6Al4V thin struts produced via SLM, coupling experimental and computational approaches. This is a preliminary but fundamental step in the design process of orthopedic patient-specific implants. In particular, the reference application of this work is an implant for the talus substitution, as discussed by the authors research group (Danielli, Berti, et al., 2023).

2. Materials and Methods

2.1. Design and fabrication of the material specimens

Cylindrical specimens were designed as shown in Fig. 1a. A diameter of 0.6 mm was chosen based on both the minimum printable dimension (0.2 mm) (Yang et al., 2021), and an average thickness of bone trabeculae (0.2 mm-1 mm) (Ho et al., 2013; Turunen et al., 2020). The samples were manufactured at the CNR-ICMATE laboratories (Lecco, Italy) using SLM technology. A Renishaw AM400 printer was exploited, and a biomedical grade Ti6Al4V ELI powder was used as raw material (spherical particles 15-45 μm). The manufacture was conducted with a spot diameter of 70 μm at the focal point, a layer thickness (t) of 30 μm, a hatching distance (H) of 65 μm, and a laser power (P) of 200 W (pulsed-wave emission mode). Due to the laser pulsed functioning, the scanning speed (v) was calculated as the ratio between the laser point distance (75 μm) and the laser exposure time (50 μs). Therefore, the laser energy density ($E = P/(t \cdot h \cdot v)$) was calculated equal to 68 J/mm^3. The meander strategy was chosen as a scanning

strategy, and the process was carried out in a reduced build volume (78·78·55 mm^3) on a Ti-based platform. Before processing, vacuum was applied (oxygen level lower than 500 ppm), the build chamber was filled with Argon, and no preheating was applied to the build platform. Three batches of material specimens were manufactured, different for the print direction with respect to the build platform (45°, 60°, 90°, Fig. 1b). The angles were chosen based on the struts inclinations of the trabecular cells commonly used for orthopedic devices (Olivares, 2022) and compatibly with the AM limits (Yang et al., 2021). As for the latter constraint, the minimum printable inclination angle is 20°. The specimens were placed 3 mm above the build plate using supports, to ensure a better heat transfer and keep them in place during the process Additionally, a second set of supports was introduced for the 45°-samples (Fig. 1c). After the manufacture, the specimens were subjected to heat treatment (850 °C for 2 hours followed by slow cooling in furnace) to avoid, or at least minimize, the presence of residual stresses. Finally, no surface treatment was performed on the specimens (Fig. 1d).

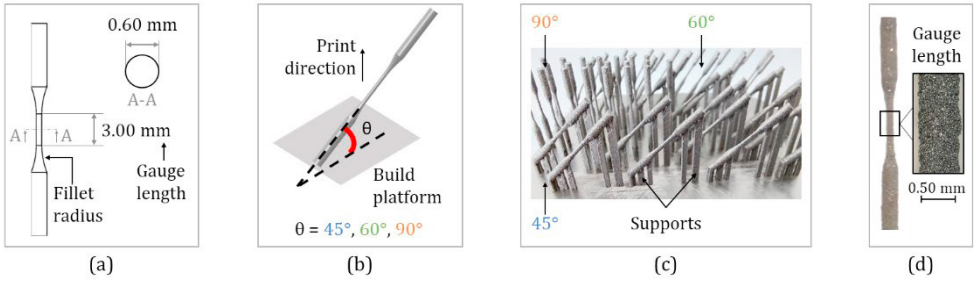

Fig. 1. (a) CAD drawing of the cylindrical samples; (b) Schematic representation of the printing process to highlight the inclination (θ) of the samples with respect to the build platform and the print direction; (c) Batches of the printed samples manufactured in Ti6Al4V through the SLM technology; (d) Example of a printed sample, with a detail about the gauge length.

2.2. Morphological characterization

The inaccuracies of AM fabrication have been outlined by the literature, and they are more evident in the presence of thin samples. In addition to the dimensions, the final product is affected by its orientation with respect to the build platform (Murchio et al., 2021a). Therefore, a deep morphological characterization is needed before performing mechanical tests. Thus, the quality of the printed samples was investigated by performing the following analyses.

- Density measurements were carried out to assess the presence of internal pores. Using the Gibertini E 50 S/2 analytical scale, the density of three samples (ρ_{SAMPLE}, g/cm^3) for each batch was calculated exploiting the Archimedes principle and compared with the one of a machined Ti6Al4V ELI alloy (ρ_{REF}, g/cm^3). From the calculated density, the porosity of the AM sample can be calculated as 1 - (ρ_{SAMPLE} / ρ_{REF}) [%].

- Lateral images were acquired with the *WILD Stereomicroscope* (7x magnification) to measure the Gauge Length (GL) of three samples for each batch and processed with the imaging software *NISELEMENTS AR Analysis* (Nikon Instruments, Melville, NY, USA);

- Profilometry analyses were performed using the *Olympus Lext Laser Microscope* (10x magnification): 2D height-maps were acquired to evaluate the surface roughness of the samples (the average roughness, R_a, was calculated). One sample for each batch was analyzed, and for each sample, the roughness of four sides was evaluated by rotating the sample of about 90° along its axis. Five measurements for each side were performed;

- Three samples for each batch were used to evaluate the cross-section; three sections for each specimen were made along the GL, 500 µm equally spaced along the specimen axis. The cut portions were embedded in epoxy resin and polished. Images were acquired using the *WILD Stereomicroscope* (32x magnification) and processed using the imaging software *ImageJ* (Wayne Rasband, National Institutes of Health, USA).

2.3. Material characterization: static tests

Static uniaxial tensile tests were performed under displacement control on three specimens for each batch until failure, using an *Instron E3000 ElectroPulse* machine. The final aim of the tests is to calculate the elastic modulus and the yield stress of the material based on the deformation of the only GL (the portion of the sample at constant cross-section, Fig. 1a), avoiding the contribution of the fillet radius (the portion of the sample at variable cross-section, Fig. 1a). Due to the small size of the specimens, extensometers could not be applied to measure the deformation of the GL. Therefore, experimental tests were coupled with numerical analyses: FE models of the samples were developed considering the actual dimensions of the samples (2.2), and the experimental tests were numerically replicated using *Abaqus/CAE 2020* (Dassault Systèmes, Vélizy-Villacoublay, France). Based on the experimental force-displacement curves and the results of the simulations, the elastic modulus (E) was calculated as follows:

$$\alpha = \frac{u_{GL}^{FEA}}{u_{TOT}^{FEA}} \qquad \varepsilon_{GL} = \frac{u_{TOT}^{EXP}}{L_0} \cdot \alpha \qquad \sigma^{EXP} = \frac{F^{EXP}}{A_0} \qquad E = \frac{\sigma^{EXP}}{\varepsilon_{GL}} \tag{1}$$

where: α is the percentage of displacement of the only GL, u_{TOT}^{FEA} is the displacement applied in the FE simulation, u_{GL}^{FEA} is the resulting numerical displacement of the GL, ε_{GL} is the deformation of the GL, u_{TOT}^{EXP} is the experimental applied displacement (the distance between the grips of the testing machine), L_0 is the GL initial length (the value was assigned based on the measures described in 2.2), σ^{EXP} is the experimental stress on the GL, F^{EXP} is the force recorded during the experimental test, A_0 is the GL initial cross-section area (the value was assigned based on the measures described in 2.2). The elastic modulus of the samples was calculated as the slope of the line interpolating the elastic portion of the stress-strain curve, and the yield stress was determined based on the 0.2% offset method: the interpolation line is offset by 0.002 of the strain and its intersection with the stress-strain curve is the yield stress.

As compared to the previous work published by the authors (Danielli, Berti, et al., 2023), the calculation of the static material properties has been performed considering not only the effective cross-section area of the manufactured samples but also their effective gauge length, which was previously assumed to be equal to the nominal dimension.

2.4. Material characterization: preliminary fatigue tests

Tensile-tensile fatigue tests were performed under force control using an *Instron E3000 ElectroPulse* machine with the following parameters: load ratio $0 < F_{MIN}/F_{MAX} < 1$, mean force F_{MEAN}=40 N, frequency f=60 Hz. Since this was a preliminary investigation, fatigue tests were conducted to construct only the finite life fatigue curve of Wöhler diagram, following the ISO 12107 standard (ISO 12107:2012, 2012). Moreover, only the 60°- and the 90°-samples were tested. Three load levels were considered for both batches, and five specimens were tested for each level.

Tests were conducted until either specimen failure or runout ($5 \cdot 10^5$). The runout was chosen based on the final aim of the project within which the current study falls: the design of a talus prosthesis. Considering the walking activity as a cyclic load and assuming an average of 10^6 steps/year, the time needed to reach an almost fully-osteointegration of the implant is about half a year ($5 \cdot 10^5$ cycles), during which it is reasonable to assume that the prosthesis is the only element bearing the body weight, without the support of the surrounding bone tissue. This condition represents the worst-case scenario to be investigated during the fatigue analysis. Finally, Scanning Electron Microscope (SEM) images of the fracture surfaces were acquired using a *Zeiss LEO 1430 SEM* (300x magnification). Two surfaces were analyzed for each batch, one for the highest load level and one for the lowest.

3. Results

3.1. Morphological characterization

The density measures showed no significant differences among the three batches (4.33 ± 0.01 g/cm^3), leading to an overall samples porosity with respect to a fully solid machined Ti6Al4V ELI (density of 4.42 g/cm^3) of 2%. The measurements of the GL outlined a significant mismatch with respect to the length in the nominal model (3 mm, Fig. 2a). Namely, the relative difference was found to increase with the increase of the sample inclination: about 40% for

the 45°-sample and about 60% for the 90°-sample. The results of the profilometry analysis were analyzed by distinguishing between the samples downskin and upskin surfaces. The former is the surface directed towards the build platform, while the latter is the 180°-opposite one. This distinction can be made for inclined samples, while no differentiation can be made for the vertical samples since no lateral surface faces the build platform. The relative difference between the downskin surface roughness and the upskin one was higher for the 45°-samples (the upskin is about 55% less rough than the downskin) with respect to the 60°-ones (the upskin is about 40% less rough as compared to the downskin). For both the 45°- and 60°-samples, the surface roughness of the other two surfaces fell within the range defined by the downskin and upskin surfaces. As for the 90°-samples, no significant differences were found for the four lateral views, and the average surface roughness fell within the range defined by the downskin and upskin surfaces of the 45°- and 60°-samples (Fig. 2c). Finally, the actual cross-section areas underrated the nominal one (0.283 mm^2). The lower relative difference was found for the 45°-samples (3%), while the higher one for the 90°-samples (20%). Besides the values, the shapes were observed. The mismatch from the nominal circular shape was found to increase as the sample inclination decreased. The 90°-samples exhibit an almost circular shape, the 45°-samples a drop-like shape with the tip in the downskin surface, while the 60°-samples an intermediate shape (Fig. 2b).

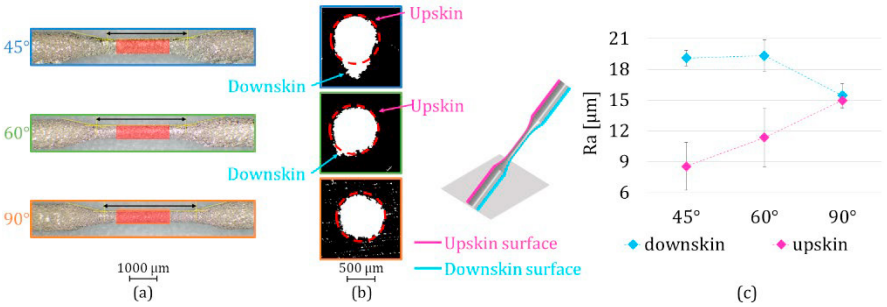

Fig. 2. (a) Actual gauge lengths (black lines) compared with the nominal ones (red rectangles); (b) Actual cross-sections (white images) compared with the nominal ones (dashed red lines). The downskin and upskin surfaces are highlighted for the 45°- and 60°-samples; (c) Average surface roughness (R_a) measured on the upskin and downskin surfaces (45°- and 60°-samples), and on two arbitrary surfaces (90°-samples).

3.2. Material characterization: static tests

The results of the static tensile tests are reported in Fig. 3: for each batch, the average stress-strain curves out (Fig. 3c) of three tests were derived from the experimental force-displacement (Fig. 3b) curves and were used for the calculation of the elastic modulus and the yield stress (Table 1). The tests performed on the same sample batches are repeatable, as shown by the slight standard deviation (vertical black lines) of both the force-displacement and stress-strain curves. Moreover, no significant differences exist among the stress-strain curves for the different batches.

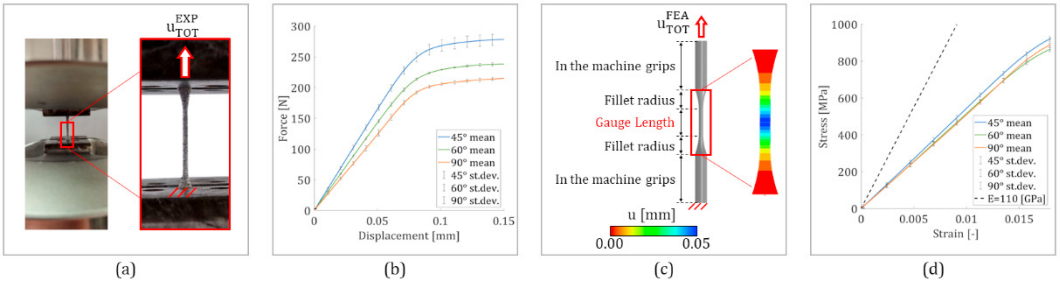

Fig. 3. (a) Static tensile test; (b) Force-displacement curves recorded during the experiments: average values and standard deviations; (c) Simulation of the experiment with a detail of the displacement field in the gauge length and in the filler radii; (d) Stress-strain curves for the gauge length: average values and standard deviations. The dashed black line is representative of the mechanical behavior of both thick AM Ti6Al4V samples (Material Data Sheet - SLM Ti6Al4V ELI, n.d.) and machined Ti6Al4V samples (Material Data Sheet - Ti6Al4V ELI, n.d.).

The quantitative results of the analyses reported in paragraphs 3.1 and 3.2 are summarized in Table 1.

Table 1. Main results obtained from the morphological analyses and from the static tests for each samples batch.

Quantity	45°-sample	60°-sample	90°-sample
Density [g/cm^3]	4.327±0.043	4.320±0.030	4.3240±0.031
Gauge length [mm]	4.307±0.219	4.781±0.129	4.908±0.184
Ra side 1 [µm] – Downskin	19.106±0.750	19.333±1.530	15.462±1.126
Ra side 2 [µm]	18.028±1.625	19.886±2.961	15.157±0.766
Ra side 3 [µm]	14.118±2.991	19.082±3.116	14.362±0.748
Ra 4 side [µm] – Upskin	8.557±2.329	11.352±2.810	14.993±0.765
Cross-section area [mm^2]	0.276±0.011	0.253±0.005	0.221±0.011
Elastic modulus [GPa]	72.9±2.3	70.2±2.2	69.1±2.8
Yield Stress [MPa]	968.1±28.9	898.7±3.5	936.5±17.9

3.3. Material characterization: preliminary fatigue tests

The results of the fatigue tests and the reconstructed finite life fatigue curve of Wöhler diagram are shown in Figure 4a. SEM images of the fracture surfaces are shown in Figure 4b. The tear zone (yellow dashed line) is located near the upskin surface for the 45°- and 60°-samples, while no preferential areas are identified for the 90°-samples. The red arrows indicate potential crack nucleation sites.

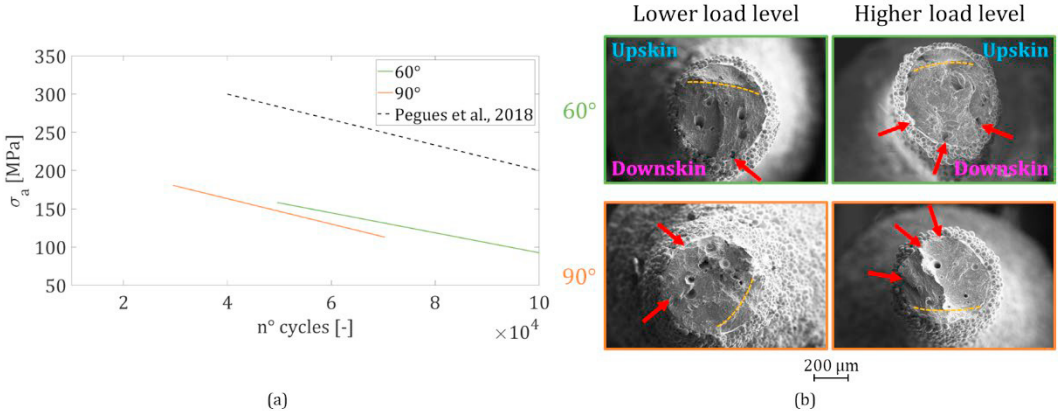

Fig. 4. (a) Finite life fatigue curve of Wöhler diagram (alternating stress as function of the number of cycles) for 60°- and 90° samples. The dashed black line is representative of the mechanical behavior of thick AM Ti6Al4V samples (Pegues et al., 2018); (b) Fracture surfaces at the lower and higher load levels. The dashed yellow lines delineate the tear surfaces, while the red arrows indicate potential crack nucleation sites.

4. Discussion and conclusions

AM has been recognized with great potential in the personalized medicine industry. It is currently a well-established technology for the production of lattice-based orthopedic prostheses. The trabeculae involved in the lattice structures are characterized by small dimensions that approach the accuracy limit of AM technologies, hindering a high-fidelity manufacture of the structures with respect to the conceived model. Many works in the literature clearly state how the final AM product may present several defects, such as internal porosity and surface roughness. Based on this evidence, they aim to study the peculiarities of AM production by investigating geometry and mechanical behavior of the final product. However, very few works focused on the characterization of thin struts, and a comprehensive overview of

their characterization is still lacking. Thus, the current study aimed to raise the main issues in the characterization of thin struts by proposing a pipeline fitting in the context of designing an orthopedic prosthesis.

Starting from the morphological analyses, the samples density was measured to estimate the presence of internal pores. The results are in line with works that studied the influence of AM process parameters on the occurrence of defects in Ti6Al4V samples, finding an internal porosity of 1%-5% (Gong et al., 2015; Khorasani et al., 2019).

As for the dimensional measurements, the discrepancy between the nominal and the actual length of the GL (more than 40%) is an issue not raised by the literature, despite its relevance in the material characterization. For instance, the authors of the current work did not question the effective GL in their recent work (Danielli, Berti, et al., 2023), leading to a misinterpretation of the experimental tests and a wrong calculation of the elastic modulus of the previously tested samples, which still belonged to the same batches of the specimens of the current study. On the contrary, the mismatch of the cross-section areas (5%-20% lower with respect to the nominal one) and the surface roughness (in the range of 14-17 μm) are evidence pointed out by the works in the literature (Murchio et al., 2021a), whose results are in line with the ones obtained in the current work. Moreover, these quantities are affected by the sample inclination with respect to the build platform. For instance, as the inclination decreases (e.g., 45°), the cross-section areas assume a "drop-like" shape, where the elongated portion is directed towards the build platform. Moreover, the difference in the surface roughness between the downskin and the upskin surfaces is more evident for lower-angle samples. Both evidences can be attributable to not optimal heat dissipation and gravitational force during the printing process.

The results obtained from the morphological analyses highlight how the nominal model produced of an AM sample cannot be considered for further investigations, such as FE analyses, especially if its dimensions approach AM accuracy limit. Moreover, the morphology of the final product is strictly affected by the sample inclination with respect to the build platform.

Looking at the static tests, the primary outcome was a decrease of about 40% for the elastic modulus with respect to both thick AM Ti6Al4V samples (*Material Data Sheet - SLM Ti6Al4V ELI*, n.d.) and machined Ti6Al4V samples (*Material Data Sheet - Ti6Al4V ELI*, n.d.): an average value of 70 GPa was obtained in contrast with 110 GPa-120 GPa. The observed reduction is consistent with the literature findings (Danielli, Ciriello, et al., 2023; Dzugan et al., 2018; Murchio et al., 2021a). For instance, both (Dzugan et al., 2018) and (Murchio et al., 2021b) characterized SLM Ti6Al4V samples (0.6 mm diameter), obtaining an elastic modulus of about 60 GPa and 80 GPa, respectively. Thus, it is possible to state that the results reported in the current work fall within the literature range. Finally, the authors did not find significant differences among the 45°-, 60°- and 90°-samples, suggesting that the print direction does not affect the elastic modulus. The wrong assumption on the dimension of the gauge length in (Danielli, Berti, et al., 2023) led to an apparent dependence of the elastic modulus from the inclination, which the current results have disclaimed.

The results of the fatigue tests outlined a reduction of 20%-40% for the limit stress within $5 \cdot 10^4$-10^5 cycles with respect to the results of (Nakatani et al., 2019; Pegues et al., 2018), in which SLM Ti6Al4V samples (3 mm-6 mm diameter) were tested. Moreover, the results of the current work agree with the study of (Murchio et al., 2021a), where the limit stress within $5 \cdot 10^4$-10^5 cycles was about 100-180 MPa for 90°-samples (L-PBF Ti6Al4V samples with 0.6 diameter). Looking at the SEM images of the fracture surfaces, it is reasonable to assume that for the 60°-samples, the tear zone is close to the upskin surface, while the source for the crack propagation is close to the downskin surface. On the contrary, the 90°-samples do not show specific areas as possible sources of crack nucleation. However, how the surface roughness affects the fatigue life of AM thin samples needs to be deeply investigated.

To conclude, AM uncertainties in producing thin struts and their effect on the morphology and mechanical properties are currently unclear. The preliminary finding of the current study aimed to highlight the main related issues by proposing a methodology for their evaluation. Looking at the biomedical context, a deep insight into geometrical and material properties of these structures is crucial in view of correctly describing the mechanics of AM lattice-based prostheses. Moreover, this is an unavoidable task if FE models are used as predictive tools of the implants behavior.

References

Danielli, F., Berti, F., Nespoli, A., Colombo, M., Villa, T., La Barbera, L., & Petrini, L. (2023). Towards the development of a custom talus prosthesis produced by SLM: design rules and verification. *Journal of Mechanical Science and Technology*. https://doi.org/10.1007/s12206-022-2109-z

Danielli, F., Ciriello, L., La Barbera, L., Rodriguez Matas, J. F., & Pennati, G. (2023). On the need of a scale-

dependent material characterization to describe the mechanical behavior of 3D printed Ti6Al4V custom prostheses using finite element models. *Journal of the Mechanical Behavior of Biomedical Materials*, *140*. https://doi.org/10.1016/j.jmbbm.2023.105707

Dzugan, J., Seifi, M., Prochazka, R., Rund, M., Podany, P., Konopik, P., & Lewandowski, J. J. (2018). Effects of thickness and orientation on the small scale fracture behaviour of additively manufactured Ti-6Al-4V. *Materials Characterization*, *143*(April), 94–109. https://doi.org/10.1016/j.matchar.2018.04.003

Edwards, P., & Ramulu, M. (2014). Fatigue performance evaluation of selective laser melted Ti-6Al-4V. *Materials Science and Engineering A*, *598*, 327–337. https://doi.org/10.1016/j.msea.2014.01.041

Gong, H., Rafi, K., Gu, H., Janaki Ram, G. D., Starr, T., & Stucker, B. (2015). Influence of defects on mechanical properties of Ti-6Al-4V components produced by selective laser melting and electron beam melting. *Materials and Design*, *86*, 545–554. https://doi.org/10.1016/j.matdes.2015.07.147

Greitemeier, D., Dalle Donne, C., Syassen, F., Eufinger, J., & Melz, T. (2016). Effect of surface roughness on fatigue performance of additive manufactured Ti–6Al–4V. *Materials Science and Technology (United Kingdom)*, *32*(7), 629–634. https://doi.org/10.1179/1743284715Y.0000000053

Ho, J. T., Wu, J., Huang, H. L., Chen, M. Y. C., Fuh, L. J., & Hsu, J. T. (2013). Trabecular bone structural parameters evaluated using dental cone-beam computed tomography: Cellular synthetic bones. *BioMedical Engineering Online*, *12*(1). https://doi.org/10.1186/1475-925X-12-115

Hossain, U., Ghouse, S., Nai, K., & Jeffers, J. R. T. (2021). Mechanical and morphological properties of additively manufactured SS316L and Ti6Al4V micro-struts as a function of build angle. *Additive Manufacturing*, *46*, 102050. https://doi.org/10.1016/j.addma.2021.102050

ISO 12107:2012. (2012).

Khorasani, A. M., Gibson, I., Awan, U. S., & Ghaderi, A. (2019). The effect of SLM process parameters on density, hardness, tensile strength and surface quality of Ti-6Al-4V. *Additive Manufacturing*, *25*, 176–186. https://doi.org/10.1016/j.addma.2018.09.002

Material Data Sheet - SLM Ti6Al4V ELI. (n.d.). https://www.slm-solutions.com/fileadmin/Content/Powder/MDS/MDS_Ti-Alloy_Ti6Al4V__ELI_0719_EN.pdf

Material Data Sheet - Ti6Al4V ELI. (n.d.). https://www.upmet.com/sites/default/files/datasheets/ti-6al-4v- eli

Murchio, S., Dallago, M., Zanini, F., Carmignato, S., Zappini, G., Berto, F., Maniglio, D., & Benedetti, M. (2021a). Additively manufactured Ti–6Al–4V thin struts via laser powder bed fusion: Effect of building orientation on geometrical accuracy and mechanical properties. *Journal of the Mechanical Behavior of Biomedical Materials*, *119*(March), 104495. https://doi.org/10.1016/j.jmbbm.2021.104495

Murchio, S., Dallago, M., Zanini, F., Carmignato, S., Zappini, G., Berto, F., Maniglio, D., & Benedetti, M. (2021b). Additively manufactured Ti–6Al–4V thin struts via laser powder bed fusion: Effect of building orientation on geometrical accuracy and mechanical properties. *Journal of the Mechanical Behavior of Biomedical Materials*, *119*. https://doi.org/10.1016/j.jmbbm.2021.104495

Nakatani, M., Masuo, H., Tanaka, Y., & Murakami, Y. (2019). Effect of Surface Roughness on Fatigue Strength of Ti-6Al-4V Alloy Manufactured by Additive Manufacturing. *Procedia Structural Integrity*, *19*, 294–301. https://doi.org/10.1016/j.prostr.2019.12.032

Olivares, M. A. (2022). *Design, modeling and characterization of lattice structures for orthopedic implant applications*.

Pegues, J., Roach, M., Scott Williamson, R., & Shamsaei, N. (2018). Surface roughness effects on the fatigue strength of additively manufactured Ti-6Al-4V. *International Journal of Fatigue*, *116*, 543–552. https://doi.org/10.1016/j.ijfatigue.2018.07.013

Persenot, T., Burr, A., Martin, G., Buffiere, J. Y., Dendievel, R., & Maire, E. (2019). Effect of build orientation on the fatigue properties of as-built Electron Beam Melted Ti-6Al-4V alloy. *International Journal of Fatigue*, *118*, 65–76. https://doi.org/10.1016/j.ijfatigue.2018.08.006

Turunen, M. J., Le Cann, S., Tudisco, E., Lovric, G., Patera, A., Hall, S. A., & Isaksson, H. (2020). Sub-trabecular strain evolution in human trabecular bone. *Scientific Reports*, *10*(1). https://doi.org/10.1038/s41598-020-69850-x

Yang, X., Ma, W., Gu, W., Zhang, Z., Wang, B., Wang, Y., & Liu, S. (2021). Multi-scale microstructure high-strength titanium alloy lattice structure manufactured: Via selective laser melting. *RSC Advances*, *11*(37), 22734–22743. https://doi.org/10.1039/d1ra02355a